

## Hydrogen Atom Abstraction Reactions of Charged Polyaromatic $\sigma$ -Radicals Related to the Active Intermediates of the Eneidyne Antitumor Drugs

Chris Petucci, Marianne Nyman, Leo Guler, and Hilikka Kenttämää\*

Contribution from the Department of Chemistry, Purdue University,  
West Lafayette, Indiana 47907-1393

Received September 26, 2001

**Abstract:** Polar effects are demonstrated to play an important role in controlling the reactivity of polyaromatic  $\sigma$ -radicals that are structurally related to the active intermediates of the eneidyne anticancer type antibiotics. This was accomplished by measuring the rate constants of hydrogen atom abstraction for novel, charged dehydroquinolines, dehydroisoquinolines, dehydrobenzenes, and dehydronaphthalenes in the gas phase by using Fourier-transform ion cyclotron resonance mass spectrometry. The reactivity trends observed for these radicals upon hydrogen atom abstraction from tetrahydrofuran and 2-methyltetrahydrofuran, simple models of deoxyribose, do not reflect differences in reaction exothermicities, radical sizes, exact location of the radical site in the ring system, or heteroatom–radical site distances. However, the reactivity trends match the trend in the calculated electron affinities of the radicals. The radicals' different electrophilicities result in variations in the reaction barrier due to different extents of polarization of the transition state. Generally, the reaction efficiencies are the greatest when the formally charged heteroatom is contained within the same ring system as the radical site. In this case, polar effects have the greatest influence on radical reactivity. Hence, insertion of a basic heteroatom (which gets protonated in biological systems) into specific locations in the polyaromatic ring system of the  $\sigma$ -biradicals, which ultimately cause cleavage of DNA exposed to the eneidyne antitumor drugs, should allow tuning of the reactivity of these radicals.

### Introduction

Radical-induced DNA degradation plays an important role in chemotherapy and carcinogenesis.<sup>1a,b</sup> The key step in many radical processes leading to DNA strand cleavages is hydrogen atom abstraction from a sugar moiety in DNA by a reactive aromatic  $\sigma$ -radical or  $\sigma,\sigma$ -biradical. Many antiviral and antitumor drugs are radical generators that cleave DNA through this mechanism.<sup>1</sup> However, little is known about the structure/reactivity relationships for the radical intermediates that are formed from these drugs. An in-depth understanding of the kinetic and thermodynamic factors that control the efficiency of their hydrogen atom abstraction reactions would benefit the rational design of antitumor drugs.<sup>2</sup>

Polar effects have been determined to influence the reactivity of the phenyl radical in both the gas phase and solution.<sup>3–7</sup> Pryor and co-workers<sup>6a</sup> showed that phenyl radicals' rates of hydrogen atom abstraction from aromatic hydrogen atom donors relative to chlorine atom abstraction from carbon tetrachloride ( $k_H/k_{Cl}$ ) are influenced by the radicals' substitution. The reactivity order

of  $p$ -tolyl < phenyl <  $p$ -bromophenyl <  $p$ -nitrophenyl radical was explained by the ability of electron-withdrawing substituents (Br, NO<sub>2</sub>) to polarize the transition state and thereby decrease its energy. Similar conclusions were made by Takayama and co-workers<sup>6b</sup> in their study of hydrogen atom abstraction from chlorinated alkanes relative to chlorine abstraction from carbon tetrachloride. The ratio of hydrogen atom abstraction to chlorine abstraction was found to increase in the order  $p$ -tolyl < phenyl <  $p$ -chlorophenyl <  $p$ -nitrophenyl radical. They concluded that increasing the electronegative character of the substituent, and

- (1) (a) Stubbe, J.; Kozarich, J. W. *Chem. Rev.* **1987**, *87*, 1107–1136. (b) Nicolaou, K. C.; Dai, W.-M. *Angew. Chem., Int. Ed. Engl.* **1991**, *30*, 1387–1416. (c) Protviel, G.; Bernadou, J.; Meunier, B. *Angew. Chem., Int. Ed. Engl.* **1995**, *34*, 746–769.
- (2) (a) Hoffner, J.; Schottelius, M. J.; Feichtinger, D.; Chen, P. *J. Am. Chem. Soc.* **1998**, *120*, 376–385. (b) Kraka, E.; Cremer, D. *J. Am. Chem. Soc.* **2000**, *122*, 8245–8264.
- (3) (a) *Free Radicals*; Kochi, J. K., Ed.; John Wiley & Sons: New York, 1973; Vol. 1. (b) *Free Radicals in Organic Chemistry*; Fossey, J., Lefort, D., Sorba, J., Eds.; John Wiley & Sons: New York, 1995.

- (4) For solution studies, see: (a) Bridger, R. F.; Russell, G. A. *J. Am. Chem. Soc.* **1963**, *85*, 3754–3764. (b) Pryor, W. A.; Guard, H. *J. Am. Chem. Soc.* **1964**, *86*, 1150–1152. (c) Fu, J.-J. L.; Bentrude, W. G. *J. Am. Chem. Soc.* **1972**, *94*, 7710–7722. (d) Scaiano, J. C.; Stewart, L. C. *J. Am. Chem. Soc.* **1983**, *105*, 3609–3614. (e) Sommeling, P. M.; Mulder, P.; Louw, R.; Avila, D. V.; Luszyk, J.; Ingold, K. U. *J. Phys. Chem.* **1993**, *97*, 8362–8364. (f) Yu, T.; Lin, M. C.; Melius, C. F. *Int. J. Chem. Kinet.* **1994**, *26*, 1095–1104.
- (5) For gas-phase studies, see: (a) Fahr, A.; Stein, S. E. *J. Phys. Chem.* **1988**, *92*, 4951–4955. (b) Chen, R. H.; Kafafi, A.; Stein, S. E. *J. Am. Chem. Soc.* **1989**, *111*, 1418–1423. (c) Kopinke, F.-D.; Zimmerman, G.; Anders, K. *J. Org. Chem.* **1989**, *54*, 3571–3576. (d) Yu, T.; Lin, M. C. *J. Phys. Chem.* **1994**, *98*, 9697–9699.
- (6) For substituted phenyl radicals, see: (a) Pryor, W. A.; Echols, J. T., Jr.; Smith, K. *J. Am. Chem. Soc.* **1966**, *88*, 1189–1199. (b) Takayama, K.; Masanori, K.; Migita, T. *Chem. Lett.* **1973**, 193–195. (c) Migita, T.; Takayama, K.; Abe, Y.; Kosugi, M. *J. Chem. Soc., Perkin Trans. 2* **1979**, 1137–1142.
- (7) (a) Li, R.; Smith, R.; Kenttämää, H. I. *J. Am. Chem. Soc.* **1996**, *118*, 5056–5061. (b) Heidbrink, J. L.; Ramirez-Arizmendi, L. E.; Thoen, K. K.; Ferra, J. J.; Kenttämää, H. I. *J. Phys. Chem. A*, in press. (c) Tichy, S. E.; Thoen, K. K.; Price, J. M.; Ferra, J. J.; Petucci, C. J.; Kenttämää, H. I. *J. Org. Chem.* **2001**, *66*, 2726–2733. (d) Thoen, K.; Smith, R. L.; Nousiainen, J. J.; Nelson, E. D.; Kenttämää, H. I. *J. Am. Chem. Soc.* **1996**, *118*, 8669–8676.

thus the polar nature of the radical, increases the rate of hydrogen abstraction relative to chlorine abstraction. Migita and co-workers<sup>6c</sup> studied the competition of hydrogen and chlorine atom abstraction from electron-donating (cyclohexane and toluene) and electron-accepting (chloroform) substrates by the phenyl and *p*-nitrophenyl radicals. The rate of hydrogen atom abstraction from cyclohexane and toluene versus chlorine atom abstraction from carbon tetrachloride was found to be greater for the *p*-nitrophenyl radical than the phenyl radical. These results agree with the studies above and suggest that the transition state for hydrogen abstraction is polarized by the electron-withdrawing *p*-nitro substituent. Interestingly, the phenyl radical abstracts a hydrogen atom from chloroform at a greater rate than the *p*-nitrophenyl radical. This result was rationalized by the electron acceptor character of this substrate and the difference in the electrophilicities of the two radicals.

The studies discussed above have provided useful knowledge on how substituents influence the reactivity of the phenyl radical. However, this work has not been extended to characterization of the reactivity of more complex aromatic  $\sigma$ -radicals, such as those related to the active intermediates of certain antitumor drugs. The influence of polar effects on the reactivity of complex aromatic  $\sigma$ -radicals has been addressed in the present study to gain a better understanding of the key structure/reactivity relationships for these important reaction intermediates.

Our experimental approach is based on the "distonic ion" method that involves the study of reactive radicals via their derivatives that carry a chemically inert charged group for manipulation by a Fourier-transform ion cyclotron resonance (FT/ICR) mass spectrometer.<sup>7</sup> Since a pure and abundant radical population can be generated in FT/ICR, the intrinsic reactivity of many unexplored aromatic radicals can be readily examined.<sup>8</sup> Systematic variation of the type and position of neutral substituents on such charged phenyl radicals has enabled us to acquire results that advance the understanding of the reactivity of phenyl radicals in the gas phase. For example, we have demonstrated that fluorine substitution increases a phenyl radical's (phosphonium charged group) rates of hydrogen atom abstraction from thiophenol, 1,4-cyclohexadiene, and tetrahydrofuran.<sup>7a</sup> The same applies to *meta*-substituents, which affect reactions via inductive effects, as opposed to previously studied *para*-substituents, which influence reactions via inductive as well as resonance effects.<sup>7b</sup> This study demonstrated that rates of hydrogen atom abstraction by *ortho*- and *meta*-substituted phenyl radicals (pyridinium charged group) from tributyltin hydride, benzeneselenol, thiophenol, and tetrahydrofuran increase in the following order for the substituted radicals: (*meta*)  $H < Br \approx Cl < CN$  (most reactive); (*ortho*)  $H < CF_3 \approx Cl \approx F$ .<sup>7b</sup> The reactivity order was rationalized by the different abilities of the substituents to stabilize the transition state by increasing its polar character. This study expands the current knowledge on polar effects by characterizing the reactivity of

new, complex aromatic  $\sigma$ -radicals with varying distances between the charged heteroatom and radical sites.

## Experimental Section

Extrel and Finnigan FT/MS model 2001 Fourier-transform ion cyclotron resonance mass spectrometers equipped with Odyssey data acquisition systems were used to carry out the experiments. The two instruments yield identical data. The Extrel instrument contains a dual cell consisting of two identical 2 in. cells aligned collinearly with the magnetic field produced by a 3 T superconducting magnet operated at about 2.7 T. The Finnigan instrument consists of a similar arrangement but is operated at 3 T. The cells are separated by a center plate called the conductance limit which contains a 2 mm center hole for ion transfer. This plate and the other trapping plates are maintained at +2 V unless stated otherwise. In the Extrel instrument, the dual-cell region is differentially pumped with two Balzer turbomolecular pumps (330 L/s) which are backed by an Alcatel 2012 mechanical pump. The dual cell of the Finnigan instrument is differentially pumped by two Edwards diffusion pumps (800 L/s) which are backed by an Alcatel 2012 mechanical pump. A nominal base pressure of less than  $1 \times 10^{-9}$  Torr was measured with ionization gauges on each side of the dual cell for both instruments.

Tetrahydrofuran, 2-methyltetrahydrofuran, *tert*-butylisocyanide, 3-bromoquinoline, 5-nitroquinoline, 6-nitroquinoline, 4-bromoisoquinoline, 5-nitroisoquinoline, 1,4-diiodobenzene, 1,3-dinitronaphthalene, and 2-methyltetrahydrofuran were obtained from Aldrich and used as received. The iodo derivatives of naphthalene (1-bromo-4-iodonaphthalene, 1,4-diiodonaphthalene, 1,5-diiodonaphthalene) and quinoline (3-iodoquinoline and 5-iodoquinoline) were synthesized by the replacement of  $NH_2$  by iodine.<sup>9</sup> The iodo derivative of 4-bromoisoquinoline was synthesized by reverse halogen exchange.<sup>10</sup> The identity and purity of all reagents were verified by mass spectrometry. Synthesized compounds were further characterized by <sup>1</sup>H NMR. The purity of tetrahydrofuran and 2-methyltetrahydrofuran were also verified by gas chromatography.

The dehydropyridine, dehydroquinolines, and dehydroisoquinolines were generated according to a multistep procedure by first introducing a substituted pyridine, quinoline, or isoquinoline into one side of the dual cell with either a heated solids probe or a Varian leak valve. Nominal sample pressures of  $2.0 \times 10^{-8}$  to  $1.2 \times 10^{-7}$  Torr of the radical precursors were maintained in the cell for all reactions. Methanol was introduced into the same side of the cell via a batch inlet and subjected to electron ionization (30 eV). The ions formed were allowed to react for approximately 2 s with the substituted pyridine, quinolines, and isoquinolines to protonate these radical precursors. The charged phenyl and naphthyl radical precursors were generated by reaction of 3-fluoropyridine with either a dihalobenzene radical cation or dihalonaphthalene radical cation formed by electron ionization. For example, 1,4-diiodobenzene was introduced via an unheated solids probe, and the 3-fluoropyridine nucleophile was introduced from a batch inlet into the same cell. This mixture was subjected to electron ionization (typically a 30 eV electron energy, 5  $\mu$ A filament current, and 50 ms ionization time) to produce an abundant signal for the diiodobenzene radical cation. This radical cation was allowed to react with the 3-fluoropyridine nucleophile for approximately 2 s to produce a charged, substituted iodobenzene via *ipso*-substitution of one of the iodine atoms by 3-fluoropyridine.<sup>11</sup>

The undesired ions formed by electron ionization in the other side of the cell were ejected by applying a potential of -2 V to the remote trapping plate of this cell for 10–15 ms. The protonated pyridine,

(8) For other mass spectrometric studies on related charged radicals, see for example: (a) Yu, S. J.; Hollman, C. I.; Rempel, D. L.; Gross, M. L. *J. Am. Chem. Soc.* **1993**, *115*, 9676–9682. (b) Lavorato, D. J.; Terlouw, J. K.; McGibbon, G. A.; Dargel, R. K.; Koch, W.; Schwarz, H. *Int. J. Mass Spectrom.* **1998**, *179/180*, 7–14. (c) Gerbaux, P.; Van Haverbeke, Y.; Flammang, R. *Int. J. Mass Spectrom.* **1999**, *184*, 39–47. (d) Gerbaux, P.; Barbieux-Flammang, M.; Terlouw, J. K.; Flammang, R. *Int. J. Mass Spectrom.* **2001**, *206*, 91–93. (e) Flammang, R.; Barbieux-Flammang, M.; Le, H. T.; Gerbaux, P.; Elguero, J.; Nguyen, M. T. *Chem. Phys. Lett.* **2001**, *347*, 465–472.

(9) Lucas, H. J.; Kennedy, E. R. In *Organic Syntheses*; Blatt, A. H., Ed.; John Wiley & Sons: New York, 1943; p 351.  
(10) Yang, S. H.; Li, C. S.; Cheng, C. H. *J. Org. Chem.* **1987**, *52*, 691–694.  
(11) (a) Thölmann, D.; Grützmacher, H.-F. *J. Am. Chem. Soc.* **1991**, *113*, 3281–3287. (b) Thölmann, D.; Grützmacher, H.-F. *Org. Mass Spectrom.* **1989**, *24*, 439–441.

quinolines, isoquinolines, benzene, and naphthalene radical precursors were transferred into the other side of the cell by grounding the conductance limit for approximately 130  $\mu$ s. After transfer, C–Br and C–NO<sub>2</sub> bonds on protonated 3-bromoquinoline and 5- and 6-nitroquinoline were cleaved by irradiation with 266 nm light of a Nd:YAG laser (5–10 pulses, 1.5 mJ/pulse) focused at the center hole of the conductance limit plate.<sup>12</sup> The ions were allowed to cool for 1 s by IR light emission and by collisions with neutral molecules that were present in the cell. C–I bonds, and in some cases C–NO<sub>2</sub> bonds, were cleaved by sustained off-resonance irradiation/collision-activated dissociation (SORI/CAD)<sup>13</sup> for 0.2 s at an excitation frequency 0.8–1.0 kHz greater than the cyclotron frequency of the ions. SORI/CAD was implemented by introducing argon ( $1 \times 10^{-5}$  Torr peak pressure) through a pulsed valve assembly. Prior to reactions, the desired reactant ions were isolated by ejecting all the unwanted ions from the cell by applying stored waveform inverse Fourier-transform excitation pulses (Extrel FTMS SWIFT module) to the excitation plates of the cell.<sup>14</sup> The isolated radicals were allowed to undergo reactions with selected neutral reagents for a variable period of time (typically 0.25–120 s). After reaction, the ions were excited for detection by using “chirp” excitation at a bandwidth of 2.65 MHz and sweep rate of 3200 Hz/ $\mu$ s. All the measured spectra were background reaction corrected as described earlier.<sup>7</sup> The background reaction spectrum, collected in the absence of the reactive ion of interest, was subtracted from the reaction spectrum to remove peaks not associated with the isolated ion and its reaction products. Each spectrum is the average of at least 10 transients recorded as 64k data points with one zero fill prior to Fourier transformation.

The reactivity of each radical toward tetrahydrofuran, 2-methyltetrahydrofuran, and *tert*-butylisocyanide was studied under the conditions described above. The branching ratios of the different reaction channels were derived from the constant abundance ratios of the corresponding product ions at short reaction times. The second-order reaction rate constants ( $k_{\text{reaction}}$ ) were determined under pseudo-first-order conditions from the decay of the relative reactant ion abundance as a function of time. The precision of the rate constant measurements is better than  $\pm 10\%$  (the absolute accuracy is estimated to be  $\pm 50\%$ ). The collision rate constants ( $k_{\text{collision}}$ ) were calculated using a parameterized trajectory theory.<sup>15</sup> The reaction efficiencies ( $k_{\text{reaction}}/k_{\text{collision}}$ ) were corrected for the sensitivity of the ion gauge to tetrahydrofuran, 2-methyltetrahydrofuran, and *tert*-butylisocyanide and for the pressure gradient between the cell and ion gauge. The latter correction factors were obtained by measuring the rates of reference reactions that are assumed to proceed at the collision rate for each neutral reagent (i.e., highly exothermic, barrierless reactions, such as electron transfer between the carbon disulfide radical cation and each neutral substrate or proton transfer between protonated ethanol and each neutral substrate).<sup>16</sup>

Density functional theory calculations were performed with the Gaussian 98, revision A7, suite of programs.<sup>17</sup> The geometries of dehydroquinoline, dehydroisoquinolines, dehydroben-

zenes, and dehydronaphthalenes were optimized at the B3LYP/6-31(d) + ZPVE level of theory. The optimized structures were verified to correspond to an energy minimum by calculating their vibrational frequencies (no imaginary frequencies). The zero-point vibrational energies were calculated from frequencies at the same level of theory and scaled by a factor of 0.9806 to account for the systematic overestimation of the vibrational frequencies by this density functional method.<sup>17</sup> The energies obtained for each radical after geometry optimization were converted to 298 K. To obtain the calculated vertical electron affinities of **a–f** (Table 3), the geometries of the charged radicals (B3LYP/6-31+G(d) + ZPVE) were used directly in single-point calculations. Single-point calculations of the zwitterions formed by addition of an electron to the LUMO of each charged radical were performed at the B3LYP/6-31+G(d)//B3LYP/6-31+G(d) + ZPVE level of theory. The vertical electron affinities of **h–i** (Table 6) were obtained in the same way at the B3LYP/6-31+G(d)//B3LYP/6-31G(d) + ZPVE level of theory.

## Results and Discussion

**Synthesis of Charged Heteroaromatic Radicals.** The charged radicals were synthesized in a dual-cell FT/ICR mass spectrometer by using a multistep procedure.<sup>7</sup> The charged radicals **a–f** (Figure 1) were generated by chemical ionization with methanol followed by photodissociation to cleave C–Br and C–NO<sub>2</sub> bonds. SORI/CAD was used to cleave C–I bonds and C–NO<sub>2</sub> bonds in some experiments that used 5- and 6-nitroquinoline (Scheme 1). Radicals **h–i** (Figure 2) were synthesized from dihalobenzene or dihalonaphthalene radical cations by *ipso*-substitution<sup>10</sup> of an iodine or a bromine by 3-fluoropyridine, pyridine, or quinoline, followed by cleavage of a C–I bond with SORI/CAD (Scheme 2).<sup>7,9</sup> Since bromine and pyridine have the same mass, fluoro-substituted pyridine was used in the synthesis of dehydroquinolines and dehydronaphthalenes when bromine was the leaving group. The fluorine substituent does not affect reactivity, as indicated, for example, by the similar reaction efficiencies (within experimental error) measured for **i** (23%) and the analogous phenyl radical containing a pyridine charge group (20%) upon cyano radical abstraction from *tert*-butylisocyanide. Further proof is given by the similar efficiencies of hydrogen atom abstraction from tetrahydrofuran by these radicals (0.30%).

**General Considerations of the Gas-Phase Reactivity of Charged Aromatic  $\sigma$ -Radicals.** Gas-phase reactions that occur in high vacuum are free from solvation effects except for the solvation of the ionic reactant by the neutral reagent to form the initial collision complex. Ion–dipole and ion–induced dipole forces lower the potential energy of the complex. The excess rotational and vibrational energy of this complex can be used to overcome barriers along the reaction coordinate. The rates of gas-phase ion–molecule reactions are usually governed by the energy difference ( $\Delta E$ ) between the separated reactants and the transition state corresponding to the reaction bottleneck (Figure 3).<sup>18</sup> As  $\Delta E$  increases, the reaction rate increases until at some point it reaches the collision rate (every collision leads to a reaction). After this point, the reaction will no longer be sensitive to barrier-lowering effects. Exothermic and slightly endothermic reactions occur at observable rates in our experiments.<sup>5b–d</sup> Even though the radical reactions studied here are calculated to be exothermic (–22 to –27 kcal/mol), the

(12) Thoen, K. K.; Pérez, J.; Ferra, J. J.; Kenttämä, H. I. *J. Am. Soc. Mass Spectrom.* **1998**, *11*, 1135–1140.

(13) Gauthier, J. W.; Trautman, T. R.; Jacobson, D. B. *Anal. Chim. Acta* **1991**, *246*, 211–225.

(14) Chen, L.; Wang, T.-C. L.; Ricca, T. L.; Marshall, A. G. *Anal. Chem.* **1987**, *59*, 449–454.

(15) Su, T.; Chesnavich, W. J. *J. Chem. Phys.* **1982**, *76*, 5183–5185.

(16) (a) Bartmess, J. E.; Georgiadis, R. M. *Vacuum* **1983**, *33*, 149–153. (b) Miller, K. J.; Savchick, J. A. *J. Am. Chem. Soc.* **1979**, *101*, 7206–7213.



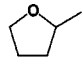
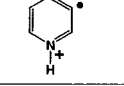
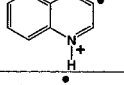
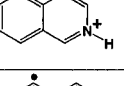
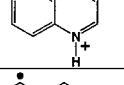
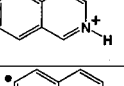
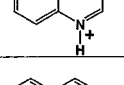
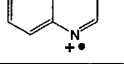
(17) Frisch, M. J.; Trucks, G. W.; Schlegel, H. B.; Scuseria, G. E.; Robb, M. A.; Cheeseman, J. R.; Zakrzewski, V. G.; Montgomery, J. A., Jr.; Stratmann, R. E.; Burant, J. C.; Dapprich, S.; Millam, J. M.; Daniels, A. D.; Kudin, K. N.; Strain, M. C.; Farkas, O.; Tomasi, J.; Barone, V.; Cossi, M.; Cammi, R.; Mennucci, B.; Pomelli, C.; Adamo, C.; Clifford, S.; Ochterski, J.; Petersson, G. A.; Ayala, P. Y.; Cui, Q.; Morokuma, K.; Malick, D. K.; Rabuck, A. D.; Raghavachari, K.; Foresman, J. B.; Cioslowski, J.; Ortiz, J. V.; Stefanov, B. B.; Liu, G.; Liashenko, A.; Piskorz, P.; Komaromi, I.; Gomperts, R.; Martin, R. L.; Fox, D. J.; Keith, T.; Al-Laham, M. A.; Peng, C. Y.; Nanayakkara, A.; Gonzalez, C.; Challacombe, M.; Gill, P. M. W.; Johnson, B. G.; Chen, W.; Wong, M. W.; Andres, J. L.; Head-Gordon, M.; Replogle, E. S.; Pople, J. A. *Gaussian 98*, Gaussian, Inc.: Pittsburgh, PA, 1998.

(18) Barfknecht, A. T.; Dodd, J. A.; Salomon, K. E.; Tumas, W.; Brauman, J. I. *Pure Appl. Chem.* **1984**, *56*, 1809–1818.





**Table 1.** Reaction Efficiencies (Eff =  $k_{\text{reaction}}/k_{\text{collision}}$ ) Determined for Protonated 3-Dehydropyridine, 3-, 5-, and 6-Dehydroquinolines, and 4- and 5-Dehydroisoquinolines upon Interaction with *tert*-Butylisocyanide, Tetrahydrofuran, and 2-Methyltetrahydrofuran<sup>a</sup>

Radical				
	a	• CN abstr. (97) HCN abstr. (3) Eff. = 86%	33	38
	b	• CN abstr. (91) HCN abstr. (9) Eff. = 75%	25	30
	c	• CN abstr. (93) HCN abstr. (7) Eff. = 73%	22	28
	d	• CN abstr. (92) HCN abstr. (8) Eff. = 49%	9	16
	e	• CN abstr. (98) HCN abstr. (2) Eff. = 53%	8	13
	f	• CN abstr. (90) HCN abstr. (10) Eff. = 48%	2	5
	g	• CN abstr. (20) HCN abstr. (71) H abstr. (9) Eff. = 65%	19	33



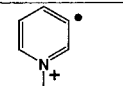
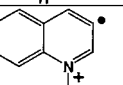
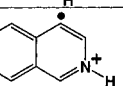
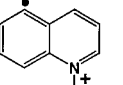
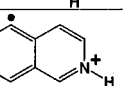
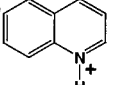
<sup>a</sup> Cyano radical and hydrogen cyanide abstraction from *tert*-butylisocyanide and hydrogen atom abstraction from tetrahydrofuran and 2-methyltetrahydrofuran were the only reactions that were observed. Relative product abundances are given in parentheses.

ions can be separated into ionic reactions occurring at the charge site, radical reactions occurring at the radical site, and reactions involving both sites.<sup>19a-d</sup> In a previous study, we demonstrated that *tert*-butylisocyanide can be used to distinguish between distonic ions with reactive and inert charge sites.<sup>19d</sup> Ions that contain a reactive charge site react with this reagent by cyanide ion abstraction, hydrogen cyanide abstraction, or proton transfer. In contrast, ions containing an inert charge site react only by cyano radical abstraction.

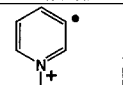
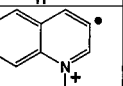
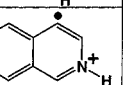
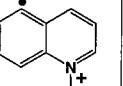
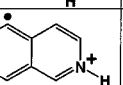
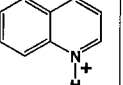
Radicals **a–f** and **h–l** abstract mainly cyano radical from *tert*-butylisocyanide (Tables 1 and 4). In contrast to the above, the conventional radical cation **g** reacts by hydrogen cyanide, cyano radical, and hydrogen atom abstraction, with hydrogen cyanide abstraction as the major pathway. Therefore, **a–f** and **h–l** are most likely distonic ions. However, because of the small amount of HCN abstraction observed for **a–f**, a small percentage of these ions may isomerize to the conventional radical cation within the collision complex. Additional support for the distonic nature of **a–f** is found by examination of the reaction efficiencies of hydrogen atom abstraction from tetrahydrofuran by these ions and the conventional radical cation **g**. Cation **g** reacts with tetrahydrofuran at an efficiency of 19% (Table 1). The efficiencies of **b** (25%), **d** (9%), and **f** (2%) are quite different.

**Summary of Hydrogen Atom Abstraction Reactions of Charged Aromatic  $\sigma$ -Radicals.** Radicals **a–f** and **h–l** were allowed to react with tetrahydrofuran and 2-methyltetrahydrofuran, which resulted in exclusive hydrogen atom abstraction

**Table 2.** Calculated Heats of Reaction (B3LYP/6-31G(d) + ZPVE) at 298 K for Hydrogen Atom Abstraction from the 2-Position of Tetrahydrofuran and 2-Methyltetrahydrofuran by 3-Dehydropyridine, 3-, 5-, and 6-Dehydroquinolines, and 4-, and 5-Dehydroisoquinolines

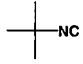

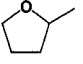
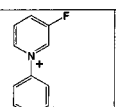
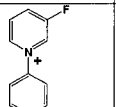
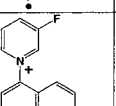
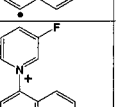
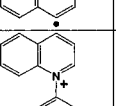
Radical			
		$\Delta H$ (kcal/mol)	$\Delta H$ (kcal/mol)
	a	-26.0	-27.5
	b	-25.8	-27.3
	c	-24.8	-26.3
	d	-23.1	-24.6
	e	-22.9	-24.4
	f	-22.8	-24.3

**Table 3.** Calculated Vertical Electron Affinities (B3LYP/6-31+G(d) + ZPVE) and Heteroatom–Radical Site Distances (through  $\sigma$ -Bonds and through Space, B3LYP/6-31G+(d) + ZPVE) of Dehydropyridine, Dehydroquinolines, and Dehydroisoquinolines

Radical		EA (eV)	Distance (Å) (through $\sigma$ -bonds)	Distance (Å) (through space)
	a	6.12	2.72	2.32
	b	5.84	2.71	2.32
	c	5.78	2.73	2.32
	d	5.21	4.21	3.65
	e	5.07	5.56	4.15
	f	4.90	5.57	4.09

by each radical (Tables 1 and 4). Reaction efficiencies for certain radicals decrease as the protonated heteroatom–radical site distance increases. For example, the reaction efficiency of **b** (25%, tetrahydrofuran) with a separation of one carbon between the protonated heteroatom and radical site is greater than that for **d** (9%, tetrahydrofuran) with a separation of two carbons

**Table 4.** Reaction Efficiencies ( $\text{Eff} = k_{\text{reaction}}/k_{\text{collision}}$ ) Determined for the Charged Dehydrobenzenes and Dehydronaphthalenes upon Interaction with *tert*-Butylisocyanide, Tetrahydrofuran, and 2-Methyltetrahydrofuran<sup>a</sup>

Radical		 Efficiency (%)	 Efficiency (%)	 Efficiency (%)
	h	29	1.1	4.0
	i	22	0.30	1.0
	j	18	0.27	0.80
	k	17	0.31	1.0
	l	20	0.29	0.62


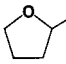
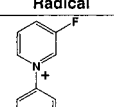
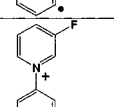
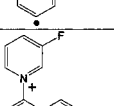
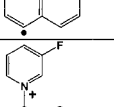
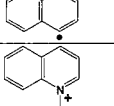
<sup>a</sup> Cyano radical abstraction from *tert*-butylisocyanide and hydrogen atom abstraction from tetrahydrofuran and 2-methyltetrahydrofuran were the only reactions that were observed.

between each site. The same trend applies to **h** compared to **i–l** (charge and radical sites on different ring systems) although their reaction efficiencies ( $\sim 0.03$ –1%, tetrahydrofuran) are lower than those of **a–f** (2–33%, tetrahydrofuran). However, the reactivity of other groups of radicals does not follow the trend noted above. For example, the reaction efficiencies of **a–c** with tetrahydrofuran (**a**, 33%; **b**, 25%; **c**, 22%) differ even though their protonated heteroatom–radical site distances (Table 3) are the same. The same deviation occurs for **e** and **f** with tetrahydrofuran (**e**, 8%; **f**, 2%). Furthermore, radicals **d** and **e** have similar reaction efficiencies with tetrahydrofuran (**d**, 9%; **e**, 8%) but different protonated heteroatom–radical site distances. Finally, radicals **i–l** have similar charged heteroatom–radical site distances (Table 6) and very similar reaction efficiencies with tetrahydrofuran ( $\sim 0.30\%$ ).

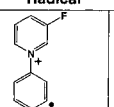
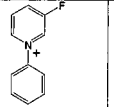
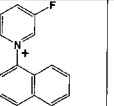
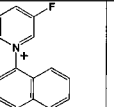
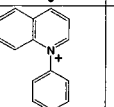
The same reactivity trends were observed for 2-methyltetrahydrofuran. However, the efficiencies of hydrogen atom abstraction from 2-methyltetrahydrofuran by **a–f** and **h–l** are greater than those for tetrahydrofuran. This result is rationalized in the discussion on polar effects given below.

**Influence of Reaction Exothermicities on Barriers for Hydrogen Abstraction.** The exothermicities of hydrogen atom abstraction from tetrahydrofuran and 2-methyltetrahydrofuran by **a–f** and **h–l** were calculated at the B3LYP/6-31G(d) + ZPVE level of theory to examine the origins for the differences observed in reaction efficiencies for these radicals (Tables 2 and 5; the same values were obtained for a few test cases at the higher B3LYP/6-311++G(d,p) level of theory). For these calculations, hydrogen atom abstraction from position 2 was assumed for both hydrogen atom donors because molecular

**Table 5.** Calculated Heats of Reaction (B3LYP/6-31G(d) + ZPVE) at 298 K for Hydrogen Atom Abstraction from the 2-Position of Tetrahydrofuran and 2-Methyltetrahydrofuran by Charged Dehydrobenzenes and Dehydronaphthalenes

Radical		 $\Delta H$ (kcal/mol)	 $\Delta H$ (kcal/mol)
	h	-22.1	-23.6
	i	-22.2	-23.7
	j	-21.7	-23.2
	k	-21.6	-23.1
	l	-21.9	-23.4

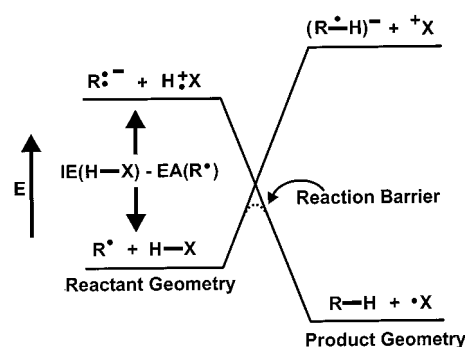
**Table 6.** Calculated Vertical Electron Affinities (B3LYP/6-31+G(d)//B3LYP/6-31G(d) + ZPVE) and Heteroatom–Radical Site Distances (through  $\sigma$ -Bonds and through Space, B3LYP/6-31G(d) + ZPVE) of Dehydrobenzenes and Dehydronaphthalenes

Radical		EA (eV)	Distance (Å) (through $\sigma$ -bond)	Distance (Å) (through space)
	h	5.05	4.23	3.69
	i	4.68	5.62	4.15
	j	4.60	5.60	4.17
	k	4.65	5.72	4.90
	l	4.46	5.62	4.16

orbital calculations (B3LYP/6-31G(d) + ZPVE) revealed that removal of a hydrogen atom at the 2-position of each molecule produces the most stable radical. The calculated enthalpy changes for hydrogen atom abstraction from tetrahydrofuran by

**a–f** and **h–l** range from  $-21.6$  to  $-26.0$  kcal/mol and those for 2-methyltetrahydrofuran from  $-23.1$  to  $-27.5$  kcal/mol. Even though the overall decrease in the exothermicities throughout these series of radicals may appear to reflect the decrease in reaction efficiencies, the differences in reaction efficiencies between the radicals are too large to be accounted for by the small difference in exothermicities. For example, the calculated exothermicities of hydrogen atom abstraction from tetrahydrofuran by **a** and **b** are essentially identical (**a**,  $-26.0$  kcal/mol; **b**,  $-25.8$  kcal/mol) despite the observable difference in their reaction efficiencies (**a**, 33%; **b**, 25%). Furthermore, reaction efficiencies measured for **d–f** range from 2% to 9% (**d** > **e** > **f**), but the calculated exothermicities are basically identical ((**d**)  $-23.1$ , (**e**)  $-22.9$ , and (**f**)  $-22.8$  kcal/mol). In the same way, reaction exothermicities ( $-21.6$  to  $-22.0$  kcal/mol, tetrahydrofuran) are nearly the same for **h–l** despite the differences in reaction efficiencies between **h** (1.1%) and **i–l** ( $\sim 0.3\%$ ). The same observations also apply to hydrogen atom abstraction from 2-methyltetrahydrofuran by **a–f** and **h–l**. The differences in reaction efficiencies for **a–f** and **h–k** with 2-methyltetrahydrofuran are greater than those for tetrahydrofuran (Tables 1 and 4). A difference in reaction exothermicities of only 1.5 kcal/mol (Tables 2 and 5) between hydrogen atom abstraction from tetrahydrofuran and 2-methyltetrahydrofuran by these radicals is unlikely to account for the range of differences between their reaction efficiencies with each of these substrates. From these observations, it can be concluded that reaction exothermicity does not control the barrier heights for these reactions.

**Influence of Polar Effects on Barriers of Hydrogen Abstraction.** The large differences in reaction efficiencies observed among the radicals examined in this study can be explained by polar effects, i.e., lowering of the energy of the transition state by an increase in its polar character.<sup>5,20,21</sup> This reactivity paradigm has been used by Pross and co-workers<sup>20</sup> to describe barrier height control in radical abstraction reactions with a valence bond model based on an avoided crossing between the singlet and triplet bonding and antibonding states of reactants and products. According to this model, barrier heights are controlled mainly by bond strengths, and ionic configurations are treated as a perturbation. Donahue and co-workers<sup>21a</sup> described the formation of a barrier in electrophilic radical abstraction reactions by the avoided crossing of the ground state and ionic excited states of the reactants and products (Figure 4). According to this model, the ionic surface is not treated as a perturbation but couples strongly with the ground-state surface. Of the two models, Donahue's ionic curve crossing paradigm appears most appropriate to describe barrier heights in our work because the radicals studied here are highly electrophilic due to the presence of an electron-withdrawing positively charged group. The ionic curve crossing model is illustrated in Figure 4 for the reaction of a charged radical  $R^\bullet$  with a hydrogen atom donor  $H-X$ . The ionic configuration at the reactant geometry that most strongly contributes to the electronic structure of the transition state can be represented by  $[R^-][HX^+]$ . The ionic configuration lowers the reaction barrier at the transition-state geometry by mixing with the



**Figure 4.** Ionic curve crossing diagram describing the origin of the transition state for the reaction of an electrophilic radical with a hydrogen atom donor. The ionization energy (IE) of the hydrogen atom donor ( $H-X$ ) and the electron affinity (EA) of the radical ( $R^\bullet$ ) at the reactant geometry, and the EA of the radical after hydrogen atom abstraction ( $R-H$ ) and IE of the hydrogen atom donor after hydrogen transfer ( $X^\bullet$ ) at the product geometry, determine the energy of the ionic surface at the reactant and product geometries. In the vicinity of the crossing point, the wave function of the ionic surface couples strongly with the wave function of the ground-state surface, thus stabilizing the transition state for hydrogen atom abstraction.

transition-state wave function, which produces a lower lying, more polar transition state (see Figure 4). Both the (vertical) electron affinity (EA) of the radical and the (vertical) ionization energy (IE) of the H-atom donor contribute to the stabilization of the reactant-type ionic configuration according to  $IE_{HX} - EA_R$ .

The expected influence of polar effects on reaction efficiencies involving each substrate can be evaluated<sup>5b–d</sup> on the basis of differences in the electron affinities of the radicals. Vertical, instead of adiabatic, values were employed because they are in better agreement with the ionic curve crossing model.<sup>21a</sup> The trend in the calculated electron affinities (**a** > **b**  $\approx$  **c** > **d**  $\approx$  **e** > **f**  $\approx$  **h** > **i**  $\approx$  **j**  $\approx$  **k**  $\approx$  **l**) matches exactly the trend in the reaction efficiencies (**a** > **b**  $\approx$  **c** > **d**  $\approx$  **e** > **f**  $\approx$  **h** > **i**  $\approx$  **j**  $\approx$  **k**  $\approx$  **l**).

As the ionization energy of the hydrogen atom donor is lowered, the energy of the ionic configuration, and therefore the energy level of the avoided crossing (transition state), decreases. This phenomenon might in part explain the slight rate enhancement for reactions of **a–f** (Table 1) and **h–l** (Table 4) with 2-methyltetrahydrofuran (ionization energy 9.22 eV) as compared to tetrahydrofuran (ionization energy 9.38 eV).<sup>22</sup> Similar behavior has been noted in our laboratory in past experiments for hydrogen atom donors with a wide range of ionization energies.<sup>5c,d</sup>

**Influence of Polar Effects on Reactions of Protonated Dehydropyridine, Dehydroquinolines, and Dehydroisoquinolines.** As noted above, stabilization of the transition state for hydrogen atom abstraction by radicals **a–f** can be explained by the differences in their electron affinities. In some cases, as the heteroatom–radical site distance increases (Table 3), the electron affinities of the radicals, and hence reaction efficiencies (Table 1), decrease. For example, the lower electron affinity of **d** (5.21 eV, Table 3) explains its lower reaction efficiency with tetrahydrofuran (9%) compared to that of **b** (25%) with an electron affinity of 5.84 eV. Further increasing the protonated heteroatom–radical site distance by a change in the position of

(20) Pross, A.; Yamataka, H.; Nagase, S. *J. Phys. Org. Chem.* **1991**, *4*, 135–140.

(21) (a) Donahue, N. M.; Clarke, J. S.; Anderson, J. G. *J. Phys. Chem. A* **1998**, *102*, 3923–3933. (b) Clarke, J. S.; Kroll, J. H.; Donahue, N. M.; Anderson, J. G. *J. Phys. Chem. A* **1998**, *102*, 9847–9857.

(22) *NIST Standard Reference Data Base Number 69*; Mallard, W. G., Lindstrom, P. J., Eds.; National Institute of Standards and Technology: Gaithersburg, MD, November 1998 (<http://webbook.nist.gov>).



the heteroatom (**e**) or radical site (**f**) results in a lower electron affinity (**e**, 5.07 eV; **f**, 4.90 eV) and lower reaction efficiency with tetrahydrofuran (**e**, 8%; **f**, 2%). The difference in reaction efficiencies between **e** and **f** is due to differing electron affinities despite the fact that they both have the same protonated heteroatom–radical site distance. The difference in Mulliken charges for **e** and **f** (**e**, 0.215; **f**, 0.069) at the radical site supports the difference in their electron affinities. However, comparison of **d** and **e** demonstrates a case where a difference in the heteroatom–radical site distance (**d** < **e**) does not affect the reaction efficiency. The similar reaction efficiencies for these two radicals are due to similar electron affinities. Similarly, the reaction efficiencies for **a–c** with tetrahydrofuran (**a**, 33%; **b**, 25%; **c**, 22%) differ even though they have the same protonated heteroatom–radical site distance. This observation can be rationalized by differences in their electron affinities (**a**, 6.12 eV; **b**, 5.84 eV; **c**, 5.78 eV). The Mulliken charges for these radicals (**a**, 0.322; **b**, 0.196; **c**, 0.044) reflect their different electron affinities. The same reactivity trends also apply to 2-methyltetrahydrofuran.

**Influence of Polar Effects on Reactions of Charged Dehydrobenzenes and Dehydronaphthalenes.** The reaction efficiencies of **h–l** (Table 4) correlate with differences in their electron affinities (Table 6) just like the trend observed for **a–f**. The separation between radical and charge sites in **h** is less than that for **i–l**; therefore, **h** (efficiency 1.1%, tetrahydrofuran) is the most electrophilic (EA = 4.87 eV) and most reactive radical. Radicals **i–l**, with equivalent heteroatom–radical site distances, have similar electron affinities (**i**, 4.51 eV; **j**, 4.45 eV; **k**, 4.50 eV; **l**, 4.46 eV) and reaction efficiencies (~0.3%, tetrahydrofuran). The fact that these radicals react at the same efficiency indicates that the size of the radical does not play a role in governing its reactivity. The similar efficiencies obtained for these radicals further demonstrate that steric hindrance of the aromatic hydrogen in the 5- and 4-positions in **j** and **k**, respectively, does not greatly influence their reactivity as compared to that of **h**. In addition, comparison of **j** and **k** shows that the 1,4-separation between the charge and radical site is nearly equally strong within the same aromatic ring and between two aromatic rings. Furthermore, the difference in the charged substituents between **i–k** (3-fluoropyridine) and **l** (quinoline) does not appear to play a role in controlling radical reactivity. The reactivity trends discussed above are observed for reactions with 2-methyltetrahydrofuran as well.

**Comparison of Protonated Dehydropyridine, Dehydroquinolines, and Dehydroisoquinolines with Charged Dehydrobenzenes and Dehydronaphthalenes.** The protonated het-

eroatom in **a–f** is located in the same ring system as the radical site; however, for **h–l**, the charged heteroatom and radical site are located on different aromatic rings. Generally, reaction efficiencies are greatest when the heteroatom is contained within the same ring system as the radical site. In this case, polar effects have the greatest influence on radical reactivity. For example, the most reactive dehydroquinoline, **b** (EA = 5.84 eV), reacts at an efficiency with tetrahydrofuran that is nearly 25 times greater than that for the most reactive phenyl radical, **h** (EA = 4.87 eV). Additionally, **d** reacts with tetrahydrofuran at an efficiency that is 9 times greater than that of **h** even though these radicals have nearly the same heteroatom–radical site distance. This result is due to the difference in their electron affinities (**d**, 5.21 eV; **h**, 4.87 eV). The exceptions to these observations are **f** and **h** since their reaction efficiencies (**f**, 2%; **h**, 1.1%; tetrahydrofuran) are essentially the same despite the fact that they have different heteroatom–radical site distances (**f**, 5.57 Å; **h**, 4.23 Å). This result is rationalized by the similar electron affinities calculated for each of these radicals (**f**, 4.90 eV; **h**, 4.87 eV).

## Conclusions

The results presented here suggest that when the reaction enthalpy does not vary greatly, polarization of the transition state is a major factor in controlling the rates of hydrogen atom abstraction by charged polyaromatic  $\sigma$ -radicals. The transition-state energy, and hence the reaction efficiency, is lowered as the electron affinities (electrophilicities) of the radicals increase. For some radicals, but not for all, this depends on the distance between the heteroatom and radical sites. The reactivity of each radical toward the two hydrogen atom donors appears to be controlled by differences in their ionization energies, possibly together with reaction exothermicities. These findings are in agreement with results reported earlier for phenyl and substituted phenyl radicals<sup>5a–c</sup> in the condensed phase and for charged substituted phenyl radicals in the gas phase,<sup>5d</sup> and conform to the Anderson, Donahue, and co-workers<sup>21</sup> reactivity model for radical–molecule reactions. Polar effect control is likely to extend to the radicals responsible for the biological activity of certain antitumor drugs and, hence, may allow “tuning” of biologically significant radical reactions.

**Acknowledgment.** We thank the National Institutes of Health for financial support of this work.

JA012243C